Neuron
Article

DSCAM and DSCAML1 Function in Self-Avoidance in Multiple Cell Types in the Developing Mouse Retina

Peter G. Fuerst,[1,6] Freyja Bruce,[2] Miao Tian,[3] Wei Wei,[5] Justin Elstrott,[5] Marla B. Feller,[5] Lynda Erskine,[2] Joshua H. Singer,[3,4] and Robert W. Burgess[1,*]
[1]The Jackson Laboratory, Bar Harbor, ME 04609, USA
[2]School of Medical Sciences, University of Aberdeen, Aberdeen, AB25 2ZD, UK
[3]Department of Ophthalmology
[4]Department of Physiology
Northwestern University Feinberg School of Medicine, Chicago, IL 60611, USA
[5]Department of Molecular Cell Biology, University of California, Berkeley, Berkeley, CA 94720, USA
[6]Present address: Department of Veterinary and Comparative Anatomy, Pharmacology and Physiology, Washington State University, Pullman, WA 99163, USA
*Correspondence: robert.burgess@jax.org
DOI 10.1016/j.neuron.2009.09.027

SUMMARY

DSCAM and DSCAM-LIKE1 (DSCAML1) serve diverse neurodevelopmental functions, including axon guidance, synaptic adhesion, and self-avoidance, depending on the species, cell type, and gene family member studied. We examined the function of DSCAM and DSCAML1 in the developing mouse retina. In addition to a subset of amacrine cells, *Dscam* was expressed in most retinal ganglion cells (RGCs). RGCs had fasciculated dendrites and clumped cell bodies in *Dscam*$^{-/-}$ mice, suggesting a role in self-avoidance. *Dscaml1* was expressed in the rod circuit, and mice lacking *Dscaml1* had fasciculated rod bipolar cell dendrites and clumped AII amacrine cell bodies, also indicating a role in self-avoidance. Neurons in *Dscam* or *Dscaml1* mutant retinas stratified their processes appropriately in synaptic laminae in the inner plexiform layer, and functional synapses formed in the rod circuit in mice lacking *Dscaml1*. Therefore, DSCAM and DSCAML1 function similarly in self-avoidance, and are not essential for synaptic specificity in the mouse retina.

INTRODUCTION

Cellular recognition involves a balance of cell adhesion and repulsion that is critical for many aspects of neuronal circuit formation. The molecular cues that promote recognition and adhesion allowing synapse formation, while preventing excessive adhesion to preserve dendritic arbors and mosaic cell body spacing, are only now being determined (Galli-Resta et al., 2008; Sanes and Yamagata, 2009). Numerous adhesion/recognition systems have been explored, and a major consideration is the molecular diversity and binding specificity needed for a molecular code that labels neurons for their integration into circuits.

The Down's syndrome cell adhesion molecule, DSCAM, is an Ig super family neural CAM that is a candidate for such a code (Yamakawa et al., 1998). *Dscam*s have been extensively studied in *Drosophila*, where *Dscam1* is alternatively spliced to generate over 38,000 possible protein products, creating extensive molecular diversity (Schmucker et al., 2000). A given neuron expresses only a few (between 14 and 50) isoforms of *Dscam1* (Neves et al., 2004; Zhan et al., 2004), and distinct *Dscam1* splice forms undergo specific homophilic interaction (Wojtowicz et al., 2007). Splice-form diversity is required for *Dscam1* function, and this is well demonstrated in sensory neuron dendrite arborization, where neurites of the same cell recognize and repel one another while allowing contact with neighboring cells that express a different compliment of *Dscam1* isoforms (Chen et al., 2006; Hattori et al., 2007; Hughes et al., 2007; Matthews et al., 2007; Soba et al., 2007). Similar *Dscam1*-mediated mechanisms are used in axon branching and synaptic target recognition in *Drosophila* (Hattori et al., 2007; Hummel et al., 2003; Wang et al., 2002, 2004; Wojtowicz et al., 2004; Zhan et al., 2004; Zhu et al., 2006). A closely related *Drosophila* gene, *Dscam2*, mediates heteroneuronal recognition between the axons of L1 neurons in the visual system, preserving the columnar "tiling" of the projections into the medulla (Millard et al., 2007). Interestingly, *Dscam2* is not extensively alternatively spliced. Therefore, *Dscam* and *Dscam2* in *Drosophila* appear to mediate self-recognition, leading to repulsion and self-avoidance (Hattori et al., 2008; Schmucker and Chen, 2009).

Vertebrate *Dscams* are implicated in a number of neurodevelopmental processes, including the specificity of pre- and postsynaptic pairing and the prevention of adhesion (Fuerst et al., 2008; Yamagata and Sanes, 2008). Vertebrate genomes contain two closely related genes (*Dscam* and *Dscaml1*), and other genes such as the sidekicks (*Sdk1* and *-2*), which encode structurally similar proteins (Agarwala et al., 2001; Yamagata et al., 2002). The vertebrate genes are not subject to extensive alternative splicing, implying functional distinctions from *Drosophila Dscam1* that eliminate this requirement (Schmucker and Chen, 2009).

In the chick, *Dscam*, *Dscaml1*, *Sdk1*, and *Sdk2* promote synaptic lamination of amacrine and ganglion cell processes in the inner plexiform layer (IPL) of the retina. This lamination is an indicator of synaptic specificity, and given cell types reliably stratify processes in distinct IPL laminae, aligning with their synaptic partners. The genes above are expressed in nonoverlapping sets of cells, and the proteins localize to distinct laminae within the IPL. Depletion or ectopic expression of these genes redirects neurite lamination, consistent with these genes determining synaptic specificity (Yamagata and Sanes, 2008). These functions in the chick are consistent with *Dscam* in *Aplysia*, where it mediates synaptogenesis in cultured neurons (Li et al., 2009).

However, in *Dscam*$^{-/-}$ mice, two retinal amacrine cell populations that would normally express *Dscam* have heavily fasciculated neurites and do not maintain mosaic spacing of their cell bodies (Fuerst et al., 2008). Therefore, mouse *Dscam* appears to be serving a function more consistent with preventing homotypic adhesion and, therefore, promoting self-avoidance rather than with synaptic adhesion.

Given vertebrate *Dscam*'s disparate functions in self-avoidance/repulsion and adhesion/synaptic specificity, we considered whether mouse DSCAM may have different functions in different cell types and whether related proteins, such as DSCAM-LIKE1 (DSCAML1), may have functions other than self-avoidance. Indeed, alternative functions of *Dscam* in other parts of the nervous system are indicated by its role in axon guidance, serving as a receptor for netrin, and by its requirement in the brainstem rhythmicity circuit in some strains of mice (Amano et al., 2009; Liu et al., 2009; Ly et al., 2008). To begin to assess this, we examined retinal ganglion cell (RGC) populations in *Dscam*$^{-/-}$ mice after finding that virtually all RGCs express *Dscam* during embryonic development. In addition, we assessed retinal anatomy and synaptic connectivity in the rod circuit using a gene-trap-knockout allele of *Dscaml1*. Our conclusions are that in all retinal cell types examined, both genes are functioning similarly in self-avoidance, whereas the stratification of neurites and synaptic specificity are intact in their absence.

RESULTS

Generation of a Null *Dscaml1* Allele

The mammalian *Dscam* gene family includes *Dscam* and *Dscaml1*. The proteins share an extracellular domain structure, with ten Ig domains and six fibronectin repeats, and have >60% overall sequence identity (Figure S1A). Much of the sequence divergence is within the intracellular domain (396 amino acids for DSCAM, 440 for DSCAML1), raising the possibility that DSCAM and DSCAML1 participate in distinct intracellular signaling pathways. To evaluate the in vivo function of *Dscaml1*, and to compare it to the function of *Dscam*, we generated mice lacking *Dscaml1* expression using embryonic stem cells with a gene trap insertion in the *Dscaml1* gene, generated by the Sanger Genome Center (line CCO772).

The gene trap insertion is integrated in the third intron of the gene (Figure S1B). This gene trap intercepts *Dscaml1* splicing, creating a transcript with at most 510 base pairs (170 amino acids) of *Dscaml1* coding sequence fused to a β-gal reporter. Northern blot analysis using a probe that recognizes the 5′ end of the transcript revealed that only the shorter fusion transcript was expressed in homozygous animals (Figure S1C). Therefore, this allele, henceforth referred to as *Dscaml1*^{GT}, is a null mutation based on the absence of protein coding mRNA. The *Dscaml1*$^{GT/GT}$ mice are viable and breed as homozygotes. The mice used in this study are hybrid 129/C57BL/6J, and approximately half the homozygous pups do not survive until weaning age if the genetic background is made increasingly C57BL/6 (generation N3). The β-gal reporter was functional and was detected in photoreceptors, cell bodies in the bipolar and amacrine-containing portions of the INL, and transiently in the RGL (Figures S1D–S1H).

Expression Pattern of *Dscam* and *Dscaml1* in Mouse Retina

Dscam and *Dscaml1* expression patterns were assayed in the mouse retina to identify cell populations that may require these genes for synaptic specificity or mosaic patterning and dendrite avoidance.

Dscam expression during embryonic development was assayed by in situ hybridization. *Dscam* was widely expressed in the retinal ganglion layer (RGL) at embryonic days 12.5 (E12.5), E14.5, E17, and at postnatal day 6 (P6) (Figures 1A–1D). Double in situ hybridization with probes to *Dscam* and *Brn3b* confirmed that cells expressing *Dscam* were RGCs (Figure 1D, inset). Furthermore, both the timing and location of *Dscam* expression in the embryonic retina are consistent with RGCs, and not "misplaced amacrine cells," accounting for the widespread *Dscam* expression in the RGL.

In situ hybridization was also performed using probes to *Dscaml1* during embryonic development (Figure 1E). No transcript was detected in the retina during embryonic development, and further analysis in *Dscaml1*$^{GT/+}$ mice using the β-gal reporter detected no expression in the retina prior to postnatal day 5 (data not shown). Antibodies to β-gal labeled two bands of cells in the inner nuclear layer (INL) of the P20 retina, as well as the inner and outer segments of photoreceptors (Figure 1F). No β-gal immunoreactivity was detected in control retinas (Figure S1 and data not shown). *Dscaml1* was also widely expressed in the brain, as demonstrated by β-gal activity (Figure S2). Staining with an antibody recognizing the entire extracellular domain of human DSCAML1 labeled the synaptic inner and outer plexiform layers (IPL and OPL, Figure 1G). This immunoreactivity was reduced to background levels in the *Dscaml1*$^{GT/GT}$ retina (Figure 1H), indicating that the antibody is specific and that the mutation eliminates the protein product.

To identify the specific cell types in the inner nuclear layer that express *Dscaml1*, we double labeled *Dscaml1*$^{GT/+}$ and *Dscaml1*$^{GT/GT}$ retinas with antibodies to β-gal and markers of amacrine and bipolar populations. The INL contains ten subtypes of bipolar cells and at least 24 types of amacrine cells (Masland, 2001; Wassle et al., 2009). β-gal-positive cells in the amacrine-containing portion of the INL expressed DAB1, a marker of AII amacrine cells (Figure 1I). In 500 DAB1 immunopositive cells counted, all were also β-gal-positive, indicating that all AII cells express *Dscaml1*. In the bipolar-containing portion of the INL, cells expressing β-gal were also positive for PKCα, a marker of rod bipolar cells (RBCs) (Figure 1J). In 200

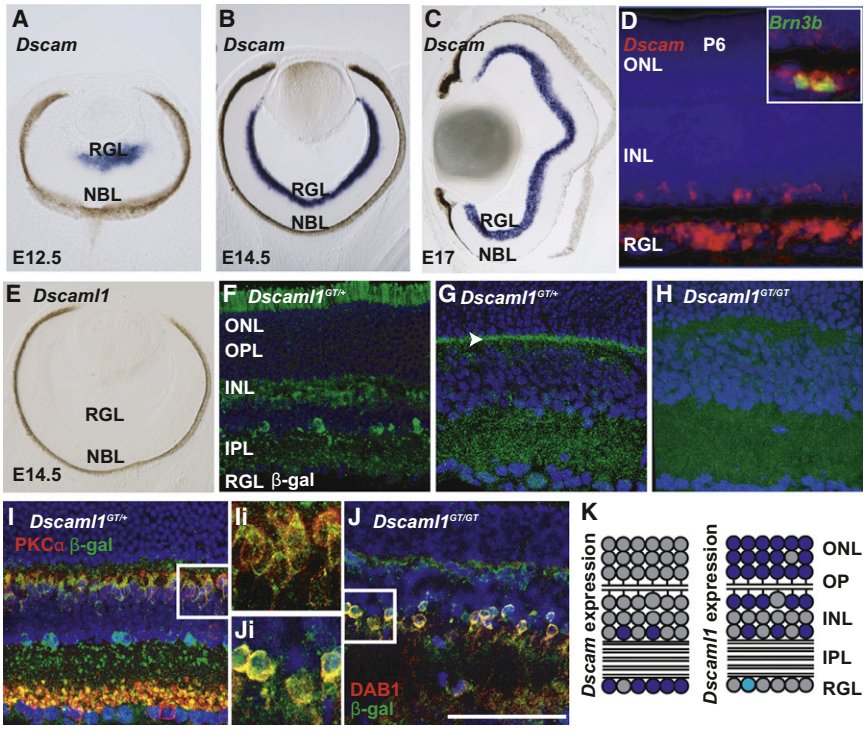

Figure 1. *Dscam* and *Dscaml1* Are Expressed in Distinct Populations of Retinal Neurons

(A–D) In situ hybridization was performed using antisense *Dscam* probes at E12.5, E14.5, E17, and P6 (inset in D is dual labeling with probes to *Dscam* and *Brn3b*). Labeling was observed in all, or nearly all, cells in the retinal ganglion cell layer (RGL) at all ages, as well as a subset of cells in the inner nuclear layer (INL) at P6. Labeling was not observed in the neuroblast layer (NBL) or outer nuclear layer (ONL).

(E) In situ hybridization was performed using antisense *Dscaml1* probes. At E14.5, no labeling was observed.

(F) Section of *Dscaml1*$^{GT/+}$ retina labeled with β-gal antibodies. Staining was observed in the inner and outer portion of the inner nuclear layer, the outer plexiform layer, and photoreceptors.

(G and H) Sections of P20 wild-type and *Dscaml1*$^{GT/GT}$ retina were stained with a polyclonal antibody to the extracellular domain of DSCAML1. DSCAML1 immunoreactivity was observed in the outer plexiform layer (OPL) and inner plexiform layer (IPL). DSCAML1 immunoreactivity was not detected in the *Dscaml1*$^{GT/GT}$ retina.

(I and J) Section of *Dscaml1*$^{GT/+}$ or *Dscaml1*$^{GT/GT}$ retina stained with antibodies to β-gal and PKCα, a marker of RBCs (I), or DISABLED1 (DAB1), a marker of AII amacrine cells (J).

(K) *Dscam* is expressed in retinal ganglion cells and some amacrine cells whereas *Dscaml1* is expressed in AII amacrine cells, RBCs, and photoreceptors.

The scale bar in (J) is equivalent to 450 μm in (A), 750 μm in (B), 900 μm in (C), 144 μm in (D), 675 μm in (E), 108 μm in (F), 90 μm in (G) and (H), 79 μm in (I) and (J), 31.6 μm in (Ii), and 27.6 μm in (Ji).

PKCα-immunopositive cells counted, all were both PKCα and β-gal immunopositive, indicating that all RBCs express *Dscaml1*. Coexpression of β-gal and other bipolar and amacrine cell markers including ChAT, TH, HCN4, calsenilin, and SYT2 was not observed (Figure S3 and data not shown). There was little or no expression in retinal ganglion cells at most ages. Occasionally, displaced DAB1-immunopositive cells were observed, contributing to a subset of cells in the ganglion cell layer that were transiently β-gal positive at P6, whereas other transiently β-gal-positive cells were also *Brn3b* positive, suggesting that they were ganglion cells (Figure S1).

The expression pattern of *Dscam and Dscaml1* in the mouse retina is therefore similar to the expression pattern of *Dscam*s in the chick retina, in that distinct cell populations express one or the other gene. However, the expression pattern is also different, in that *Dscaml1* is not widely expressed in cells in the RGL, while *Dscam* is expressed in many if not all RGCs, whereas both genes are expressed in nonoverlapping subsets of cells in the chick RGL (Yamagata and Sanes, 2008) (Figure 1K).

Dscam Is Required for RGC Dendrite Arborization and Soma Spacing

Dscam is required to prevent neurite fasciculation and maintain mosaic spacing of dopaminergic and bNOS-positive amacrine cells in the mouse retina (Fuerst et al., 2008). Retinal ganglion cell soma spacing and dendrite arborization were examined in three classes of ganglion cells for which markers were available. First, intrinsically photoresponsive ganglion cells (ipRGCs) were labeled with an antibody to melanopsin (Panda et al., 2002). Second, alpha ganglion cells, which include both "ON" cells, responding when light stimuli turn on and stratifying their dendrites in the medial portion of the inner plexiform layer, and "OFF" cells, responding when light stimuli turn off and stratifying their dendrites in the outer, scleral portion of the IPL, were labeled using the antibody SMI-32 against nonphosphorylated neurofilament. Third, a transgenic strain (Mito-Y) that expresses mitochondrially localized YFP driven by the neuron-specific enolase (NSE or *Eno2*) promoter was used to identify a third population of cells (Misgeld et al., 2007). The RGCs labeled by the Mito-Y transgene are very abundant in the dorsal portion of the retina and less abundant elsewhere in the retina (Figure S4A). Density recovery profiling (DRP) analysis, a statistical test for the probability of encountering another cell of the same type within binned distances from a reference cell body, was performed (Rockhill et al., 2000; Rodieck, 1991). The Mito-Y cells within the central and ventral retina were organized in a mosaic pattern, with an exclusion zone (an area surrounding each cell body in which other Mito-Y cells are not found) indicating that they are nonrandomly spaced (Figures S4C and S4D). All of these populations are somewhat heterogeneous and include multiple RGC subtypes. Anti-melanopsin labels both M1 and M2 ipRGCs (Schmidt and Kofuji, 2009), SMI-32 labels four classes of RGC (Coombs et al., 2006), and the Mito-Y transgenic, despite showing a mosaic pattern of cell bodies, marks at least three types of cell based on morphology and dendrite stratification (Figures S4E and S4F).

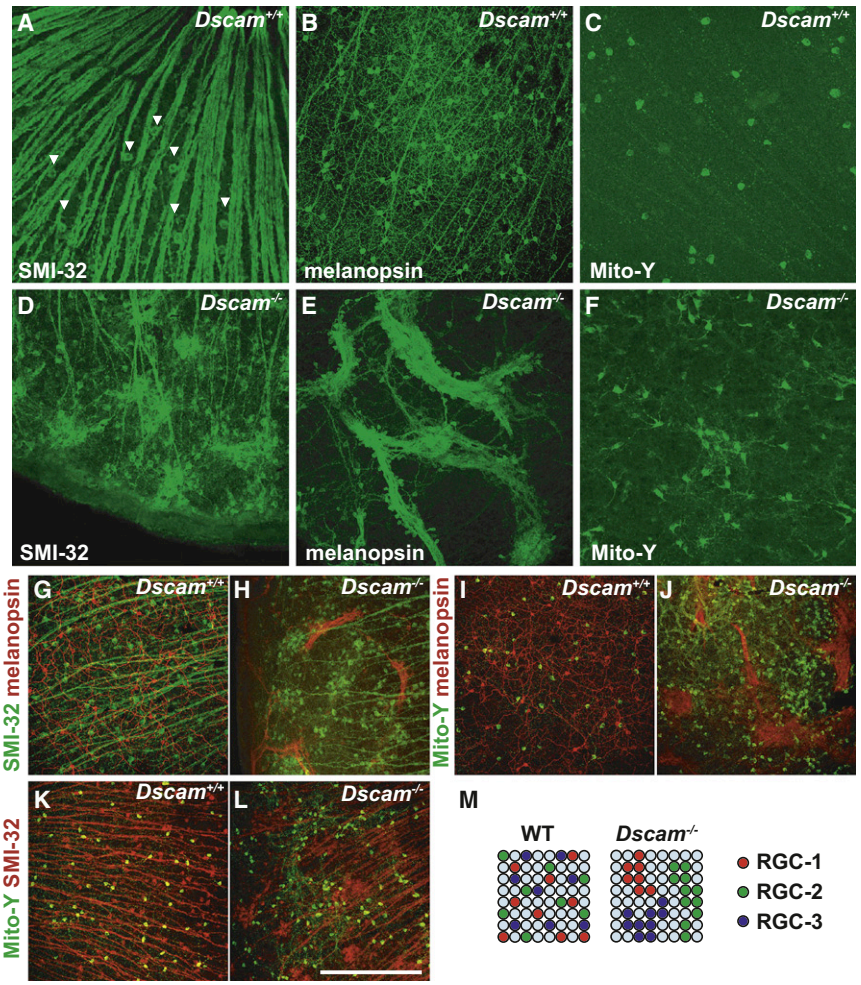

Figure 2. *Dscam* Is Required for Retinal Ganglion Cell Spatial Patterning but Does Not Confer Cell-Type Identity

Retinal ganglion cell populations were labeled in adult wild-type and *Dscam*$^{-/-}$ retinas using the antibody SMI-32 to nonphosphorylated neurofilament (A and D; alpha RGCs), anti-melanopsin (B and E; melanopsin-positive RGCs), and the Mito-Y transgene (C and F; Mito-Y-positive RGCs).

(A and D) α RGCs are aggregated in the periphery of the *Dscam*$^{-/-}$ retina compared to the wild-type retina; arrowheads denote cell bodies in the central retina of wild-type mice.

(B and E) Melanopsin-positive RGCs are densely aggregated in the *Dscam*$^{-/-}$ retina compared to wild-type. The dendrites of melanopsin-positive RGCs form fascicles in the *Dscam*$^{-/-}$ retina, whereas they arborize in wild-type.

(C and F) Mito-Y-positive RGCs are aggregated and fasciculated in the *Dscam*$^{-/-}$ retina.

(G–L) Pairwise labeling of adult wild-type and *Dscam*$^{-/-}$ retinas with antibodies to melanopsin, nonphosphorylated neurofilament (SMI-32), and the Mito-Y transgene (n > 3). RGC aggregates and fascicles in the *Dscam*$^{-/-}$ retina were composed primarily of a single RGC type (H, J, and L).

(M) RGC cell types form mosaics in the wild-type retina and aggregate and fasciculate with cells of the same type in the *Dscam*$^{-/-}$ retina.

The scale bar in (H) is equivalent to 280 μm in (A)–(F) and 387.5 μm in (G)–(L).

RGC soma spacing and dendrite arborization were disrupted in the adult *Dscam*$^{-/-}$ retina (>6 weeks of age) in each ganglion cell type examined. Alpha RGCs, labeled with SMI-32, were regularly spaced throughout the wild-type retina but were absent from the central portion of the adult *Dscam*$^{-/-}$ retina and were in dense clusters in the peripheral retina (Figures 2A and 2D). Soma spacing and arborization of melanopsin-positive ipRGCs changed from distributed cell bodies and individually arborized dendrites in the wild-type retina to clumps of cell bodies associated with thick fascicles of dendrites in the *Dscam*$^{-/-}$ retina (Figures 2B and 2E, classification as dendrites was based on MAP2 immunoreactivity and a lack of neurofilament immunoreactivity; data not shown). In contrast to wild-type, YFP-positive RGCs in the Mito-Y mice were strongly aggregated in *Dscam*$^{-/-}$ retinas (Figures 2C, 2F, S4B, and S4D). Therefore, *Dscam* is required to prevent dendrite fasciculation and promote mosaic patterning of cell bodies in RGC populations, similar to its function in amacrine cells (Fuerst et al., 2008).

Dscam Does Not Confer RGC Cell-Type Identity, but Rather Prevents Cell-Type-Intrinsic Adhesion

To determine whether cell aggregates and fascicles contained multiple cell types or consisted primarily of homotypic cells, the three RGC populations described above were examined in pair-wise combinations (Figures 2G–2L). In all cases, soma aggregation and neurite fasciculation occurred between cells of the same type, but not between different cell types, indicating that DSCAM is not required for cell type identity, but instead suggesting that an adhesive cue that is shared by all cells of a given type is unmasked in the absence of DSCAM (Figure 2M).

Dscaml1 Is Required for All Amacrine Cell Mosaic Spacing and Rod Bipolar Cell Dendrite Organization

To determine whether *Dscaml1* is involved in a similar self-avoidance function, AII amacrine and RBCs were analyzed in a *Dscaml1*$^{GT/GT}$ background. The anatomy of the retina in *Dscaml1*$^{GT/GT}$ mice was examined in histological cross-sections from P20 mice. In *Dscaml1*$^{GT/GT}$ mice, the width of the inner nuclear layer was increased and the inner plexiform layer was expanded, whereas the outer nuclear layer (photoreceptors) and retinal ganglion cell layer were unchanged compared to controls (Figures 3A–3C).

Retinas were stained with antibodies to DAB1, to label AII amacrine cells, or PKCα, to label RBCs. AII amacrine cells were disorganized in their vertical soma patterning in the *Dscaml1*$^{GT/GT}$ retina (Figures 3D and 3H). The number of AII amacrine cells was significantly increased in the *Dscaml1*$^{GT/GT}$ retina (Table 1). In an examination of whole-mount retinas, AII amacrine cells were no longer organized in the normal lateral mosaic

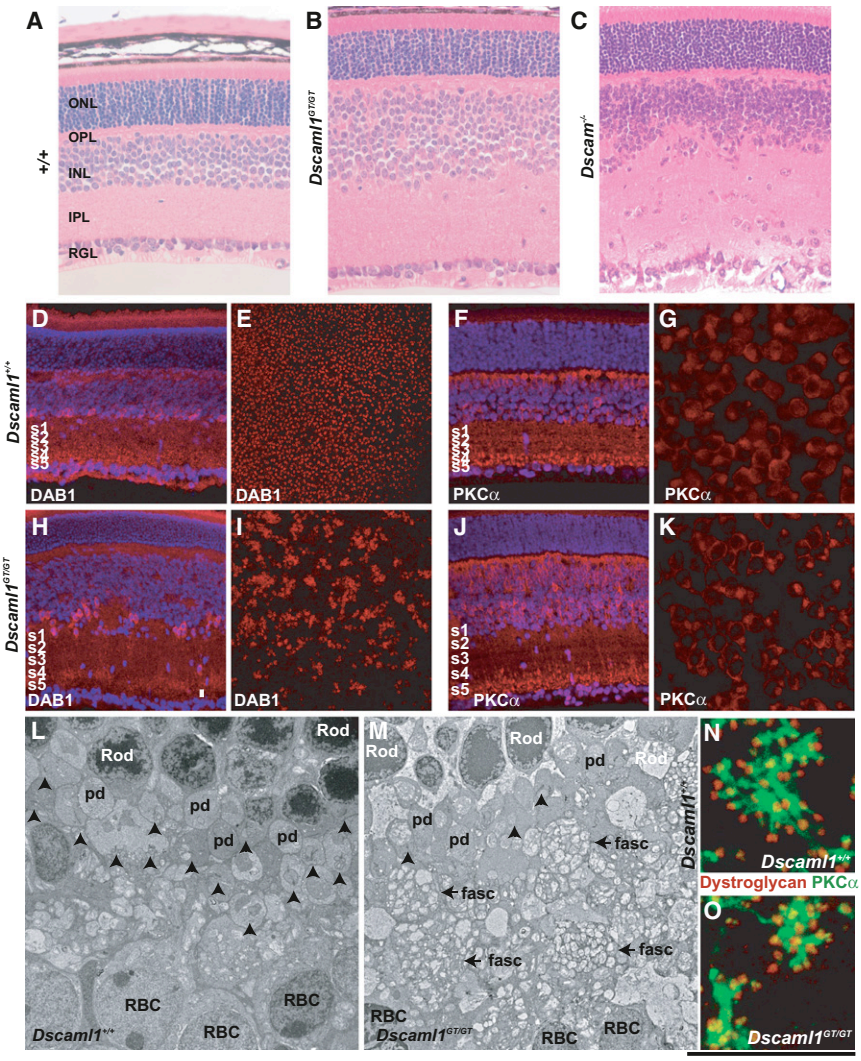

Figure 3. *Dscaml1* Is Required for Mosaic Patterning of AII Amacrine Cells and Dendritic Morphology of Rod Bipolar Cells

(A–C) Sections of wild-type, *Dscaml1*$^{GT/GT}$, and *Dscam*$^{-/-}$ retinas stained with hematoxylin and eosin. The inner nuclear and inner plexiform layers of the *Dscaml1*$^{GT/GT}$ and *Dscam*$^{-/-}$ retinas are expanded and disorganized compared to wild-type. The *Dscam*$^{-/-}$ RGL was also disorganized. No histological differences were detected between wild-type and *Dscaml1*$^{GT/+}$retinas (data not shown). Sections or whole retinas from wild-type and *Dscaml1*$^{GT/GT}$ mice were stained with antibodies to DAB1, a marker of AII amacrine cells (D, E, H, and I) or PKCα, a marker of RBCs (F, G, J, and K); ($n \geq 3$).

(D and H) AII amacrine cells in sections of wild-type and *Dscaml1*$^{GT/GT}$ retina. AII amacrine cells are clumped and vertically disorganized in the *Dscaml1*$^{GT/GT}$ inner nuclear layer compared to the regular distribution in the wild-type retina.

(E and I) AII amacrine cells are distributed in a mosaic across the surface of the inner nuclear layer of the wild-type retina but clump in the *Dscaml1*$^{GT/GT}$ retina.

(F and J) Rod bipolar cells in sections of wild-type and *Dscaml1*$^{GT/GT}$ retinas. The *Dscaml1*$^{GT/GT}$ retina has an increased number of RBCs compared to wild-type, but the synaptic termini of both wild-type and *Dscaml1*$^{GT/GT}$ RBCs are stratified in ON vitreal portion of the inner plexiform layer.

(G and K) No difference was observed when comparing the spacing of *Dscaml1*$^{GT/GT}$ and wild-type RBCs, although they are more abundant in the *Dscaml1*$^{GT/GT}$ retina.

(L and M) Transmission electron microscopy was used to examine the structure of the *Dscaml1*$^{GT/GT}$ outer plexiform layer (n = 4 mice of each genotype). The size of photoreceptor peduncles was reduced in the *Dscaml1*$^{GT/GT}$ outer plexiform layer, and fewer ribbon synapses were observed (arrows). Fascicles of rod bipolar dendrites (fasc) were also observed in the mutant retina.

(N and O) Wild-type and *Dscaml1*$^{GT/GT}$ retinas were stained with antibodies to PKCα and dystroglycan, a marker of the rod presynapse. Rod bipolar cell dendrites extend less far into the OPL in the *Dscaml1*$^{GT/GT}$ retina.

The scale bar in the lower right corner of the figure is equivalent to 156 μm in (A)–(C), 204 μm in (D), (F), (H), and (J), 664 μm in (E) and (I), 68 μm in (G) and (K), 12.75 nm in (L) and (M), and 13.5 μm in (N) and (O).

pattern observed in wild-type retinas; instead, the cell bodies adhered and aggregated in clumps (Figures 3E and 3I). Rod bipolar cells are not arranged in a mosaic pattern in the wild-type retina, and no significant difference in soma spacing was observed when comparing their distribution in the *Dscaml1*$^{GT/GT}$ retina (Figures 3F, 3G, 3J, and 3K). Rod bipolar cells were further examined by confocal imaging through different planes of the retina (Figure S5). Adhesion of RBC proximal dendrites and a significant increase in RBC number were observed in the *Dscaml1*$^{GT/GT}$ retina (Table 1).

Transmission electron microscopy was performed to examine the anatomy of the *Dscaml1*$^{GT/GT}$ retina. Dense fascicles devoid of synaptic vesicles were observed in the *Dscaml1*$^{GT/GT}$ OPL (Figures 3L and 3M; fasc). Some morphologically normal ribbon synapses were observed in the *Dscaml1*$^{GT/GT}$ OPL; however, the number of ribbons observed was reduced compared to wild-type (Table 1). A decrease in the number of ribbons was also observed at P9 and P15, indicating that the reduction is a developmental defect and not degenerative (Figure S6). Morphologies of wild-type and *Dscaml1*$^{GT/GT}$ RBCs were examined by labeling retinas with anti-PKCα, to label RBC dendrites, and anti-dystroglycan, to label the rod presynapse (Figures 3N and 3O). Rod bipolar cell dendrites extended less far in the *Dscaml1*$^{GT/GT}$ retina compared to wild-type (Table 1).

No significant difference in the number or spatial organization of cholinergic amacrine cells, horizontal cells, SMI-32-positive retinal ganglion cells, or melanopsin-positive retinal ganglion cells was observed (Figure S7 and data not shown; t test > 0.05), but DA amacrine cells were significantly increased in number in *Dscaml1*$^{GT/GT}$ mice compared to wild-type (t test < 0.02). DA cell number is influenced by genetic background, and the increase in DA cell number may be related to the

Table 1. Quantification of Wild-Type versus *Dscaml1*$^{GT/GT}$ Phenotypes

	Wild-Type	*Dscaml1*$^{GT/GT}$	T Test
All cell number/100 μm	4.4 ± 0.61	6.59 ± 2.68	0.042
Rod bipolar cells/mm^2	26,527±1008	37,031±1456	<0.005
Ribbons/100 μm OPL	47.1	13.0	N.D.
Rod bipolar cell dendrite length (μm)	1.66 ± 0.31	0.91 ± 0.20	<0.005
N.D. Not Determined			

The phenotypes of the *Dscaml1*$^{GT/GT}$ retina were quantified, including All amacrine cell number, rod bipolar cell number, ribbon synapses in the OPL, and rod bipolar cell dendrite length. Statistical significance was determined using a Student's T test.

segregating genetic background of the *Dscaml1*^{GT} allele or to the increase in All amacrine cell number (Whitney et al., 2009).

The lateral spacing of All and dopaminergic amacrine cells was examined using confocal Z projections in control and *Dscaml1*$^{GT/GT}$ whole-mount retinas (Figures 4A–4F). DRP analysis was used to assess mosaic patterning. All amacrine cells had an exclusion zone in the wild-type retina but were strongly aggregated in the *Dscaml1*$^{GT/GT}$ retina (Figures 4G and 4H). The number of All amacrine cells and the degree to which they aggregate in the *Dscaml1*$^{GT/GT}$ retina is likely to be underestimated because mutant All cells are aberrantly stacked, and therefore undercounted in confocal series. In contrast, DA cells continued to form a mosaic in the *Dscaml1*$^{GT/GT}$ retina (Figures 4I and 4J); however, their neurites were directed toward clumps of All cells, suggesting that All amacrine cells play an important role directing the patterning of the DA neurites that enwrap them.

Therefore, deletion of *Dscaml1* primarily disrupts the dendrite avoidance and mosaic patterning of those cells that express it in the wild-type retina, similar to *Dscam*. However, secondary phenotypes affecting the synaptic partners of these cell types can also be observed.

Synaptic Colamination and Specificity Is Preserved in the *Dscam* and *Dscaml1* Null Retinas

Dscams are required for synaptic lamination in the chick retina, and they are proposed to mediate synaptic specificity through adhesion (Yamagata and Sanes, 2008). We therefore examined ipRGC dendrite stratification and M1 ipRGC costratification with DA cell neurites in *Dscam*$^{-/-}$ retinas. The anti-melanopsin antibody differentiates two distinct populations of ipRGCs (Schmidt and Kofuji, 2009): M1, which stain brightly with the antibody to melanopsin, have small cell bodies and stratify in the OFF portion of the IPL, and M2, which stain dimly, have large cell bodies and stratify in the ON portion of the IPL (Figure 5A). In *Dscam*$^{-/-}$ retinas, the clumps of melanopsin-positive cells appear to be either M1 or M2 cells, based on staining intensities (Figure 5B). In cross-sections of wild-type retinas, the M1 cells costratify with the processes of dopaminergic amacrine cells at the top of the IPL (the OFF portion), and a subset of these two cell types synapse with one another (Viney et al., 2007; Zhang et al., 2008). M2 cells stratify their dendrites in the ON portion of the IPL (Figure 5C). In the *Dscam*$^{-/-}$ retina, the costratification of melanopsin-positive processes and TH-positive processes is still evident, and melanopsin-positive processes are still found in the ON portion of the IPL (Figure 5D).

To determine whether the melanopsin-positive processes in the IPL still correctly corresponded to M1 or M2 cells, we analyzed whole-mount retinas by confocal Z projections, which

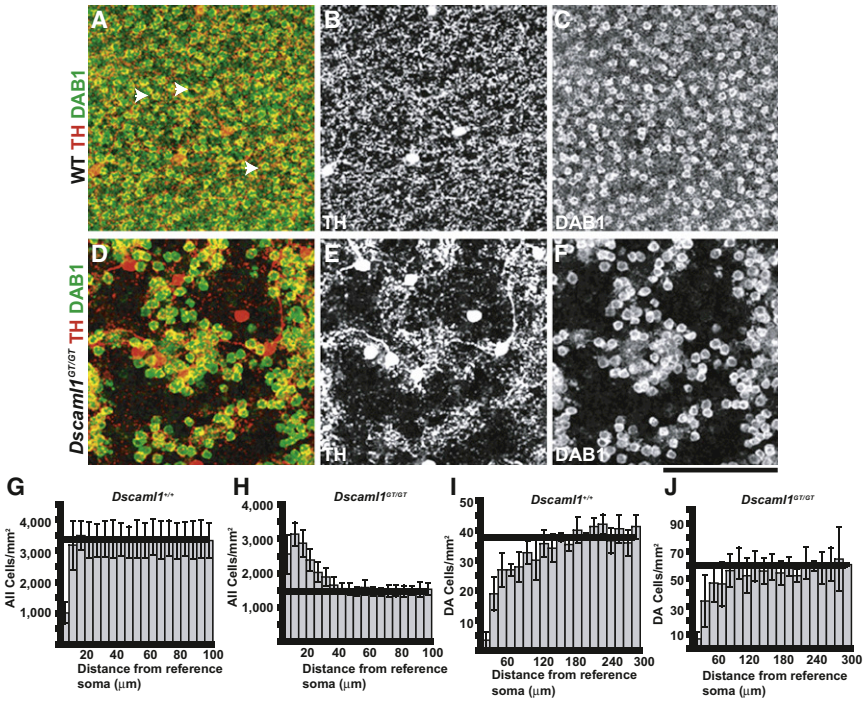

Figure 4. Analysis of Patterning of DA and All Cells

Wild-type and *Dscaml1*$^{GT/GT}$ retinas were stained with antibodies to label DA cells (TH) and All cells (DAB1).

(A–C) Spatial organization of DA and All amacrine cells form mosaics in the wild-type retina. All cells are wrapped by neurites from DA cells (arrows). Images are shown as the merge (A) and the TH (B) and DAB1 (C) signals individually.

(D–F) All amacrine cells require *Dscaml1*$^{GT/GT}$ for normal organization and clump in its absence. DA neurites are absent from areas lacking All cells (E).

(G and H) DRP analysis was performed comparing distribution of All amacrine cells in the wild-type (G) and *Dscaml1*$^{GT/GT}$ retina (H). In the wild-type retina, an exclusion zone is observed (reduction below average spacing), whereas strong aggregation is observed in the *Dscaml1*$^{GT/GT}$ retina (above average spacing).

(I and J) DRP analysis was performed comparing distribution of DA cells in the wild-type (I) and *Dscaml1*$^{GT/GT}$ retina (J). DA cells had an exclusion zone in both wild-type and *Dscaml1*$^{GT/GT}$ retina.

The horizontal lines in (G)–(J) indicate average cell densities; values are mean ± standard deviation. The scalebar below (F) is equivalent to 132 μm.

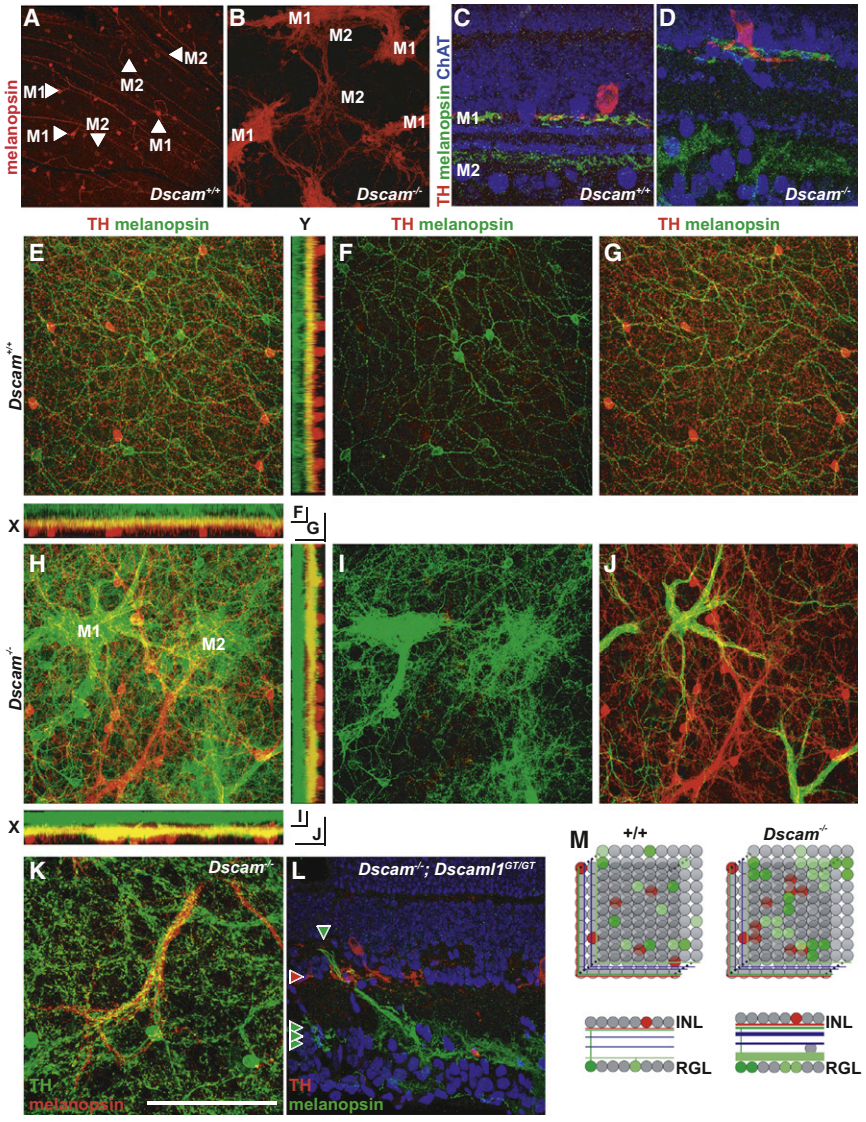

Figure 5. Confocal Projection of ipRGCs and DA Cells

Wild-type and *Dscam*$^{-/-}$ retinas were stained with antibodies to TH and melanopsin to detect DA cells and ipRGCs, respectively.

(A) Anti-melanopsin stains two populations of ipRGC, bright M1 cells and dim M2 cells in the wild-type retina.

(B) In the *Dscam*$^{-/-}$ retina, M1 and M2 cells aggregate and fasciculate separately.

(C and D) Cross-sections of wild-type and *Dscam*$^{-/-}$ retina stained with antibodies to melanopsin, TH, and ChAT. (C) In the wild-type retina, ChAT labels the neurites of cholinergic amacrine cells in the ON and OFF portion of the INL, while M1 ipRGC dendrites costratify with DA neurites immediately below the INL, and M2 dendrites stratify in the ON portion of the INL proximal to the RGL. (D) This lamination pattern is preserved in the *Dscam*$^{-/-}$ retina.

(E) A confocal Z projection from the RGL through the IPL to the amacrine cell bodies in the INL in the wild-type retina.

(F) The bottom half of the Z stack contains ganglion cell bodies and the M2 dendrites in the ON portion of the IPL.

(G) The top half contains dopaminergic amacrine cell bodies and M1 dendrites.

(H–J) In the *Dscam*$^{-/-}$ retina, melanopsin-positive dendrites stratify in two bands, with the IPL proximal band costratifying with DA neurites. (I) Dim M2 cells stratify dendrites in the ON portion of the IPL. (J) Bright M1 cell dendrites project to the IPL immediately below the INL.

(K) Cofasciculation of DA cell neurites and M1 dendrites is observed in the *Dscam*$^{-/-}$ retinas.

(L) In *Dscam*$^{-/-}$; *Dscaml1*$^{GT/GT}$ double-mutant retinas, ipRGC dendrites are fasciculated in the ON portion of the IPL, while dopaminergic amacrine neurites are fasciculated in the OFF portion of the IPL proximal to the INL; however, colamination in S1 is very disorganized.

(M) *Dscam* is required for mosaic patterning of DA and ipRGCs but gross synaptic lamination is intact.

The measurement bar in panel (K) is equivalent to 496.8 μm in (A) and (B), 64.1 μm in (C) and (D), 193.75 μm in (E)–(J), and 132 μm in (K).

were then split into the lower half (the RGL and ON strata of the IPL) and the upper half (the OFF strata of the IPL and the amacrine cell bodies). In the wild-type retina, ipRGC cell bodies and M2 dendrites, as well as M1 dendrites passing through, are present in the lower stack, whereas M1 dendrites and DA cells are present in the upper stack (Figures 5E–5G). In the *Dscam*$^{-/-}$ retina, clumps of bright ipRGC cell bodies (M1) and dimmer ipRGC cell bodies (M2) are seen in the lower stack. The dendrites of the M1 cells are fasciculated and passing through to be found in the upper stack, along with the DA processes and cell bodies, whereas the M2 dendrites are found exclusively in the lower stack (Figures 5H–5J). These results further indicate that the clumps of cell bodies observed are indeed cell type specific and also indicate that these cell types still project to appropriate strata of the IPL and costratify appropriately with other cell types. In addition to costratifying, some processes of DA and M1 ipRGCs also cofasciculated in the *Dscam*$^{-/-}$ retina (Figure 5K). This is the only example of marked cofasciculation between two different cell types observed, and it is interesting to note that these cells are synaptically coupled in the wild-type retina. Retinas from mice lacking both *Dscam* and *Dscaml1* (*Dscam*$^{-/-}$; *Dscaml1*$^{GT/GT}$) were extremely disorganized, but some degree of costratification was still present (Figure 5L). The M1 neurites projected to the OFF portion of the IPL but did not laminate along the surface of the INL. Since *Dscaml1* is not expressed in either cell population, the increased disorganization is likely to arise simply from the increased cell number in the double mutant. Therefore, *Dscam* is required for M1 ipRGC and DA mosaic patterning but not for their neurite colamination (Figure 5M).

The stratification of processes was further examined using labels for other cell populations in *Dscam*$^{-/-}$, *Dscaml1*$^{GT/GT}$

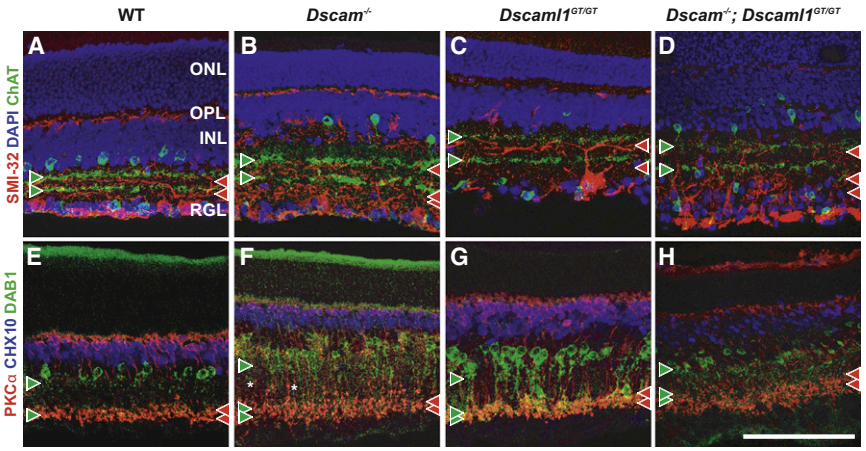

Figure 6. Synaptic Lamination Is Preserved in the *Dscam* or *Dscaml1* Null Retina

(A–D) Retina sections were stained with antibodies to ChAT to detect cholinergic Starburst amacrine cells and with SMI-32 to detect α RGCs. The location of ON and OFF cholinergic bands are used to demarcate synaptic layers S2 and S4. Paired cholinergic bands (green arrowheads) were observed in wild-type and mutant retinas, although their lamination was not as compact in the *Dscam*$^{-/-}$; *Dscaml1*$^{GT/GT}$ retina. A small number of cholinergic amacrine cell neurites were laminated in an ectopic plexiform layer within the INL of the *Dscam*$^{-/-}$; *Dscaml1*$^{GT/GT}$ retina. α RGCs stratify dendrites on the RGL proximal side of cholinergic bands (read arrow heads). Stratification proximal to cholinergic bands was observed in all genotypes, with dendrite fascicles observed in the ON portion of the *Dscam*$^{-/-}$ and *Dscam*$^{-/-}$; *Dscaml1*$^{GT/GT}$ retina.

(E–H) Retina sections were stained with antibodies to CHX10 to label bipolar cells, PKCa to label RBCs, and DAB1 to label AII amacrine cells. The axon terminals of RBCs were laminated in S4–S5 of all genotypes. Varicosities were observed in RBC axons in the *Dscam*$^{-/-}$ and *Dscam*$^{-/-}$; *Dscaml1*$^{GT/GT}$ retina. AII neurites were stratified in S1/S2 and S4/S5 of all genotypes and also colaminated with the axonal terminals of RBCs in all genotypes. All amacrine cells were observed to stratify neurites in an ectopic plexiform layer within the INL and to also project neurites past RBC terminals, toward the RGL in the *Dscam*$^{-/-}$; *Dscaml1*$^{GT/GT}$ retina. The scale bar in (H) is equivalent to 134.6 μm for all panels except (D) and (H), in which it is equivalent to 123 μm.

retinas, and in double *Dscam/Dscaml1* mutant retinas. Alpha ganglion cells were examined in combination with ChAT-positive amacrine cells. In this combination, the alpha RGCs require *Dscam,* but ChAT-positive cells do not express *Dscam* or *Dscaml1*. In a second combination, RBCs were examined with AII amacrine cells, both *Dscaml1*-expressing populations.

Alpha RGCs and cholinergic amacrine cells both laminate in distinct bands in the ON and OFF halves of the IPL in the wild-type retina (Figure 6A). Cholinergic bands mark the IPL laminae S2 and S4 (the IPL can be subdivided into five sublaminae, S1 near the INL to S5 near the RGL), and alpha RGCs laminate dendrites on the proximal (RGL) face of cholinergic bands. Paired cholinergic and alpha RGC bands are preserved in both *Dscam* and *Dscaml1* mutants; however, it is not as compact in the *Dscam* null retina (Figures 6B and 6C). The *Dscam/Dscaml1* double null retina was similar to the *Dscam*$^{-/-}$ retina (Figure 6D).

AII amacrine neurites project glycinergic terminals onto OFF cells in S1/S2 and form a synapse with RBC terminals in S5 (Figure 6E). AII amacrine cells and RBCs continue to colaminate in the ON portion of the IPL in the *Dscam*$^{-/-}$ and *Dscaml1*$^{GT/GT}$ retina (Figures 6F and 6G). The *Dscam/Dscaml1* compound mutant retina was similar to the single mutant retinas (Figure 6H).

Therefore, while synaptic lamination in *Dscam* and *Dscaml1* mutant retinas was not as sharp as that observed in the wild-type retina, neurites did continue to laminate in the proper portion (ON or OFF) of the IPL, and synaptic colamination was preserved, suggesting that *Dscams* are not required for synaptic specificity in the mouse retina.

Synapses Are Functional in the *Dscaml1* Null Retina

The expression of *Dscaml1* in the rod circuit provided the opportunity to confirm that costratification of terminals was indicative of functional connectivity between rods and RBCs, and between RBCs and AII amacrine cells (Figure 7A).

Double labeling adult retina cross-sections for AII and RBCs revealed that in addition to costratifying in the ON portion of the IPL, the terminals of the two cell types were still in close apposition in the mutant retina (Figures 7B and 7C). These cells form a "dyad" synapse, which can be identified by electron microscopy. The large (>2 μm) rod bipolar terminal forms a ribbon synapse at the junction of an AII and an A17 amacrine cell (Raviola and Dacheux, 1987). The AII cells are electron dense, and the A17 cell forms a reciprocal synapse with the RBC terminal. This anatomical arrangement was still readily evident in the *Dscaml1*$^{GT/GT}$ IPL, although the synaptic ribbons were not as well formed in the bipolar terminal, and there was an overabundance of vesicles (wild-type: 288 ± 59.44 vesicles/μm^2 versus *Dscaml1*$^{GT/GT}$: 457.1 ± 108.5 vesicles/μm^2 t test = 0.02), raising the possibility that functional exocytosis is impaired in the mutant retina (Figures 7D and 7E, n = 3 mice examined per genotype, >8 synapses per mouse, at 2 months of age).

The mutant AII-RBC synapse was functional, as determined by a comparison of paired recordings from synaptically coupled cells in slice preparations of adult control (C57BL/6) and *Dscaml1*$^{GT/GT}$ retinas. Presynaptic RBCs were depolarized from a holding potential of −50 mV to −10 mV to elicit a presynaptic Ca current (Figures 7F and 7G*i*). Presynaptic Ca^{2+} influx evoked exocytosis of glutamatergic vesicles, as indicated by the excitatory postsynaptic current (EPSC) recorded in the AII cell (Figures 7F, 7G*ii*, and 7G*iii*). Synaptic transmission was similar in *Dscaml1*$^{GT/GT}$ and wild-type mice (*Dscaml1*$^{GT/GT}$ versus wild-type): EPSC amplitude = 220.1 ± 51.2 versus 240 ± 61.0 pA, p = 0.78 by ANOVA; Ca current amplitude (measured at steady-state) = 27.8 ± 6.5 pA versus 23.4 ± 3.6 pA, p = 0.53 by ANOVA (n = 7 paired recordings from 4 *Dscaml1*$^{GT/GT}$ mice and n = 7 paired recordings from 3 wild-type mice). However, the decay of the EPSC (from peak to steady-state current) was slower in the *Dscaml1*$^{GT/GT}$ mice. A decay time constant (τ_{decay})

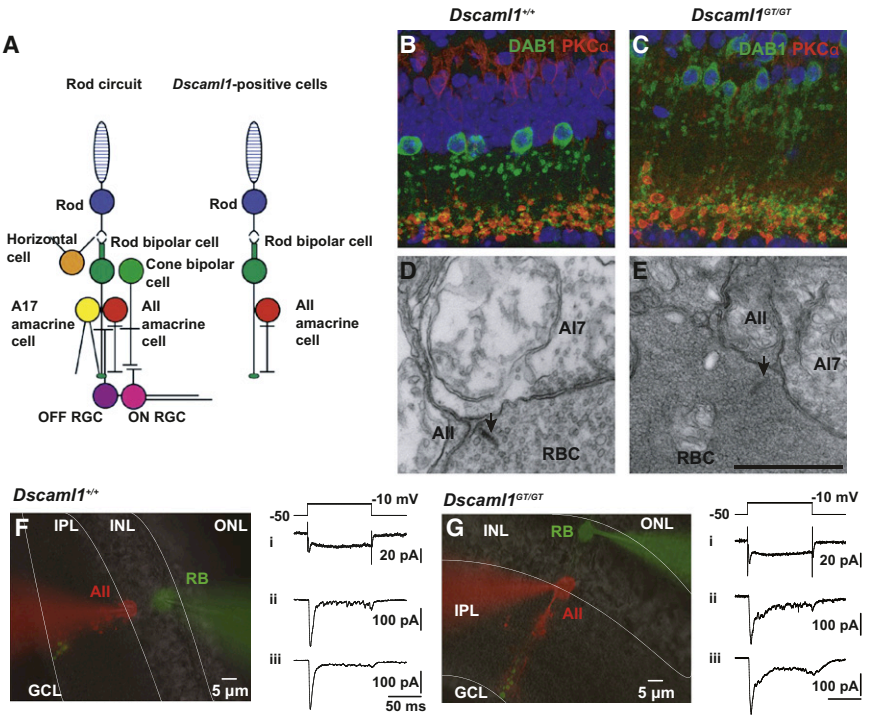

Figure 7. Rod Bipolar and AII Amacrine Cells Remain Synaptically Coupled in the *Dscaml1* Null Retina

(A) Schematic of the rod visual circuit. Light responses in the rods leads to synaptic activation of RBCs. Rod bipolar cells form a dyad synapse with A17 amacrine cells, which are inhibitory, and AII amacrine cells. AII amacrine cells form an inhibitory glycinergic synapse with OFF cone bipolar cells and RGCs and form gap junction connections with ON cone bipolar cell terminals, which transmit visual information to ON RGCs. *Dscaml1* is expressed in three cell types within this circuit: rods, RBCs, and AII amacrine cells.

(B and C) Sections of wild-type and *Dscaml1*$^{GT/GT}$ retina were stained with antibodies to disabled (DAB1) to label AII amacrine cells and with PKCα to label RBCs (n = 3). Colamination of RBC axonal terminals and AII amacrine cell neurites was observed in the inner plexiform layer proximal to the retinal ganglion cell layer. Colamination was preserved in the *Dscaml1*$^{GT/GT}$ retina, even in rare cases where the rod bipolar axon terminals were ectopically localized within the inner plexiform layer.

(D and E) Wild-type and *Dscaml1*$^{GT/GT}$ retinas were imaged by transmission electron microscopy (n = 4). Rod bipolar cells, AII amacrine cells, and A17 amacrine cells form a three-part synapse, the dyad synapse, which was observed in both wild-type and *Dscaml1*$^{GT/GT}$ retinas. *Dscaml1*$^{GT/GT}$ synapses had an overabundance of vesicles and rudimentary synaptic ribbons in bipolar cell terminals.

(F) Photomicrograph of paired recording shown with fluorescence images of the rod bipolar (green) and AII (red) superimposed over a transmitted light image of the retinal slice. In the wild-type retina, depolarization of the presynaptic rod bipolar from −50 to −10 mV elicits an inward Ca current (*i*) and evokes an EPSC in the postsynaptic AII (*ii* is an individual EPSC; *iii* is the average of seven responses).

(G) The same paired recording analyses performed in *Dscaml1*$^{GT/GT}$ mice, again showing the presynaptic bipolar cell Ca current (*i*), an individual EPSC (*ii*), and the average EPSC (*iii*), note the slower decay phase of the postsynaptic response.

The scale bar below panel (E) is equivalent to 76 μm in (B) and (C) and 1.2 μm in (D) and (E).

was calculated from either a double exponential function fit to *Dscaml1*$^{GT/GT}$ recordings (the average τ_{decay} is reported) or a single exponential function fit to wild-type recordings. τ_{decay} (*Dscaml1*$^{GT/GT}$ versus wild-type) was 7.4 ± 1.1 versus 3.6 ± 0.3 ms ($p = 0.002$ by ANOVA). The decay of the transient component of the EPSC may reflect the depletion of a small, readily releasable vesicle pool at the rod bipolar active zone (Singer and Diamond, 2006). The differences in EPSC decay between the *Dscaml1*$^{GT/GT}$ and wild-type recordings suggest differences in the number of vesicles in the rod bipolar presynaptic terminal (Figures 7D and 7E) or the time course of exocytosis. These experiments do, however, clearly indicate that the synaptic specificity between rod bipolar and AII amacrine cells is intact, and the synapses are functional, despite possible structural and functional differences from wild-type.

Synaptic connectivity between rods and RBCs in the OPL was also examined. Bassoon, a marker of the rod presynaptic density, and CACNA1S, a marker of the RBC postsynaptic site, were used to determine if synaptic specificity was intact in the *Dscaml1*$^{GT/GT}$ OPL. The number of synapses was decreased (Table 1); however, pre- and postsynaptic apposition was intact (Figures 8A and 8B). Rod bipolar cell dendrites colaminated with calbindin-positive horizontal cell axons in the outer plexiform layer (Figures 8C and 8D). Transmission electron microscopy showed that ribbon structures still formed in the *Dscaml1*$^{GT/GT}$ retina (Figures 8E–8H). Consistent with the light microscopy data, fewer ribbons were observed in the *Dscaml1*$^{GT/GT}$ retinas, and floating ribbons that were not in contact with the presynaptic membrane were also present.

Despite differences in OPL morphology, the rod-to-rod bipolar synapse was functional, as demonstrated by the robust bipolar cell response in dark-adapted electroretinograms (ERG). In dark-adapted ERGs, the initial signal in response to a light flash (the A wave) represents the activation of the rods, while the second wave (the B wave) is primarily signal from the synaptic activation of the bipolar cells. The A and B waves in *Dscaml1*$^{GT/GT}$ mice trended toward larger amplitudes compared to wild-type mice (Figures 8I, 8J, and S8). This is consistent with the increase in RBC number but may also be influenced by a decrease in the number of synapses or changes in the synaptic efficacy in the mutant, resulting an insignificant change in amplitude overall. For comparison, ERG recordings from *Dscam*$^{-/-}$ mice were also normal but with reduced amplitude compared to control (Figure 8K; n = 5 for all genotypes at ages between 2–3 months).

Therefore, *Dscaml1* is required for dendritic organization and soma patterning but is not required for synaptic specificity, and functional synapses form in its absence.

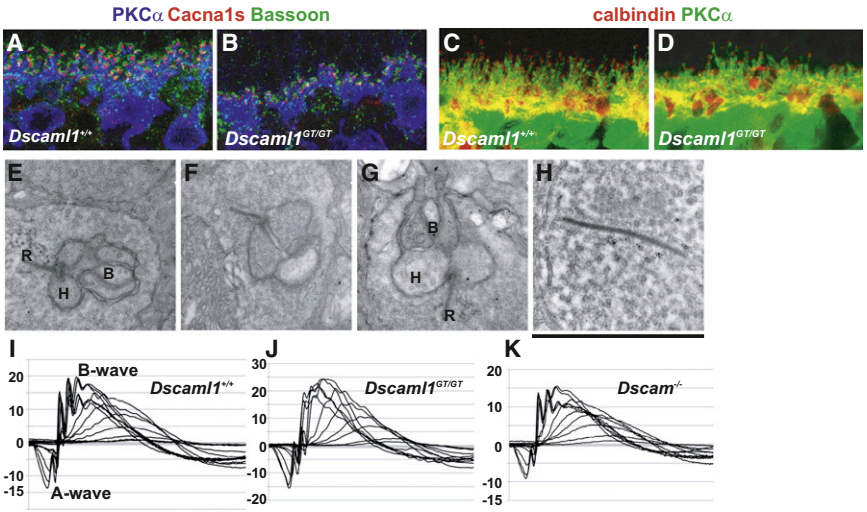

Figure 8. Rods and Rod Bipolar Cells Remain Synaptically Coupled in the *Dscaml1*$^{GT/GT}$ Retina

(A and B) Sections of wild-type and *Dscaml1*$^{GT/GT}$ retinas were stained with antibodies to PKCα to label RBCs, Bassoon, a marker of the rod presynapse, and Cacna1s, a component of the RBC postsynapse. Presynaptic and postsynaptic markers were paired in both the wild-type and *Dscaml1*$^{GT/GT}$ retina, although the number of synapses was reduced in the mutant retina.

(C and D) Sections of wild-type and *Dscaml1*$^{GT/GT}$ retinas were stained with antibodies to PKCα to label RBCs and with calbindin, a marker of horizontal cells (n = 2). The dendrites of both wild-type and *Dscaml1*$^{GT/GT}$ RBCs colaminated with horizontal cell axons.

(E–H) Transmission electron microscopy was used to examine the anatomy of the *Dscaml1*$^{GT/GT}$ ribbon synapses. Examples of ribbon synapses from wild-type (E and F) and *Dscaml1*$^{GT/GT}$ (G and H) retinas showing the photoreceptor ribbon (R) apposed to a horizontal cell (H) and invaginating bipolar cells (B, typically an ON bipolar dendrite flanked by darker OFF bipolar processes). An increase in floating ribbons was seen in the mutant (H).

(I–K) Electroretinography (ERG) was performed on wild-type, *Dscaml1*$^{GT/GT}$, and *Dscam*$^{-/-}$ mice (n ≥ 5). Rod bipolar cells receive input from rods in the *Dscaml1*$^{GT/GT}$ mice, as demonstrated by the robust B wave, reflecting postsynaptic bipolar cell activation, which had a greater amplitude compared to wild-type and *Dscam*$^{-/-}$ mice.

The scale bar below panel (H) is equivalent to 32.4 μm in (A) and (B), 40.9 μm in (C) and (D), and 478 nm in (E)–(H).

DISCUSSION

Both *Dscam* and *Dscaml1* are involved in a form of self-avoidance in the mouse retina in all cell populations we have examined. The genes have nonoverlapping expression patterns in the mouse retina, with *Dscam* being expressed in a subset of amacrine cells and most retinal ganglion cells beginning soon after these cells are born. *Dscaml1* is expressed in the rod circuit, including rod photoreceptors, RBCs, and AII amacrine cells. In the absence of either gene, the cells that would normally express it show excessive fasciculation of their dendrites and clumping of their cell bodies. Thus, in normal function, *Dscam* and *Dscaml1* appear to prevent this excessive adhesion, a role that is tantamount to the repulsive self-avoidance function seen for *Dscam*s in *Drosophila*. In contrast, the DSCAMs do not appear to be required to specify synaptic connections. The processes of *Dscam* or *Dscaml1* mutant cells still costratify with their synaptic partners in discrete laminae in the plexiform layers. In addition, the synaptic connections of the rod circuit remain functional in *Dscaml1*$^{GT/GT}$ retinas. The synapses are reduced in number and are morphologically abnormal, and DSCAML1 may play a role in finalizing the synaptic architecture, consistent with its localization, but the appropriate cells still find one another and establish functional connections in its absence.

These results indicate that the role of *Dscam*s in the mouse retina may be divergent from the role of *Dscam*s in the chick retina (Yamagata and Sanes, 2008). In this model, the cells in the inner nuclear layer use the proteins as a homophilic adhesive code to connect with appropriate RGC dendrites. This function in chick may be similar to DSCAM's role in *Aplysia*, where it is necessary for synaptogenesis in cultured motor and sensory neurons of the gill-withdrawal reflex and for later plasticity at these synapses. However, this function in synapse formation and specificity does not appear to be conserved in the mammalian retina.

Although mouse DSCAM and DSCAML1 both function in a form of self-avoidance similar to *Dscam1* and *Dscam2* in *Drosophila*, there remain important distinctions from the fly as well. In particular, mouse DSCAMs lack the extensive molecular diversity generated by the alternative splicing of *Dscam1* in the fly. In keeping with their limited repertoire, the mouse genes do not appear to be conferring cell identity. In *Drosophila*, a given cell is able to recognize its own dendrites, axon, or synaptic partners while being invisible to its neighbors, because each cell expresses only a small fraction of the possible *Dscam1* splice variants, and molecular interaction and self-avoidance are isoform specific (Neves and Chess, 2004; Neves et al., 2004).

In the mouse retina, the clumps of cell bodies and fascicles of processes that form in the absence of *Dscam* or *Dscaml1* consist largely of cells of the same type or a cell type and its synaptic partner. In this regard, it appears that DSCAMs are masking adhesive codes that are shared by cells of a given type, and in the absence of DSCAMs, these adhesive cues are unmasked. In this way, the DSCAMs effectively mediate self-avoidance and do so in the absence of molecular diversity.

The mechanisms by which DSCAMs function in this form of self-avoidance are unclear at both the cellular and molecular levels. However, some rules are apparent. The mechanism must allow for a great deal of tolerance for interactions between cells of the same type in the wild-type retina. The mosaics of mammalian retinal neurons are often not truly tiled, where each cell occupies a territory that is devoid of processes of other cells of the same type. Instead, the cell bodies are nonrandomly spaced in mosaic patterns, where an "exclusion zone" exists around each cell, preventing other cells of the same type from

residing close by, but the processes of these cells intermingle extensively, with coverage factors (the average area occupied by a cell of a given type multiplied by the number of cells of that type in that area) of 2–3 and as high as 7–9. Therefore, it is difficult to conceive of a mechanism in which the mammalian DSCAMs are actively repellent, unless this repulsion is very short range or very weak. This point is further exemplified by the expression of *Dscam* by most ganglion cells, which must interact extensively, and by *Dscaml1* expression in RBCs, a very densely packed cell type.

At this cellular level, one inviting hypothesis is that DSCAMs prevent adhesion passively, serving simply as nonstick coatings that mask the cell-type-intrinsic adhesive cues. The main attraction of this hypothesis is that it does not require extensive molecular diversity; a cell expressing *Dscam* would simply be indifferent to other cells expressing *Dscam* (or *Dscaml1* cells to other *Dscaml1* cells), unless overpowered by an appropriate adhesive signal. The presence of multiple non-stick coatings (DSCAM and DSCAML1) would allow some cell types to maintain a close association under normal circumstances, such as the processes of dopaminergic amacrine cells (*Dscam*-expressing) that encircle the cell bodies of AII amacrine cells (*Dscaml1*-expressing). Alternative mechanisms are also possible; for example, the DSCAMs may be present in a gradient with a high-proximal, low-distal concentration on the membrane of neurites. This could establish an exclusion zone around each cell body but still allow interaction of the distal processes with other cells of the same type. Unfortunately, existing anti-DSCAM antibodies lack the sensitivity and specificity needed to assess the protein distribution on the cell surface.

At the molecular level, intracellular signaling pathways must be involved. Both DSCAM and DSCAML1 are homophilic adhesion molecules when transfected into nonadhesive cell types, but mediate self-avoidance in vivo. In *Drosophila*, the intracellular domain of DSCAM1 is required for its function in self-avoidance (Matthews et al., 2007). *Drosophila* and mammalian DSCAM intracellular domains may share some signaling functions. Fly DSCAM1 interacts with PAK1 (P21 Activated Kinase) via DOK, whereas human DSCAM binds PAK1 directly (Li and Guan, 2004; Schmucker et al., 2000). PAK1 is involved in many pathways, and although PAK1 isoforms are dynamically localized in the mouse retina, we have seen little difference in PAK1 activation in the $Dscam^{-/-}$ and $Dscaml1^{GT/GT}$ retina (Figure S9). PAK1 is also not required for self-avoidance in *Drosophila*, and it may therefore be a better candidate for other DSCAM functions, such as axon guidance (Andrews et al., 2008; Hughes et al., 2007). The C termini of DSCAM and DSCAML1 also share PDZ interaction consensus sequences, suggesting that the DSCAMs may be part of a larger adhesion/signaling complex. Further examination of DSCAM signal transduction and binding partners will be required to understand these mechanisms.

How the mechanisms leading to fasciculation and clumping in the mutant retina relate to the increase in cell number of the affected cell populations is also unclear. In both *Dscam* and *Dscaml1* mutant retinas, there is an overabundance of the cell types that would normally be expressing the respective genes. In amacrine cells, increased cell number arose from decreased developmental cell death (Fuerst et al., 2008). This is true in ganglion cells as well. These cells are born embryonically and die in the first few postnatal days. In the $Dscam^{-/-}$ retina, the ganglion cell number is not different than control at E18, but is significantly increased by P5. A delayed wave of cell death ensues, partially restoring cell number by P15 (Figure S10A; data not shown). Interestingly, this effect is also sensitive to *Dscam* gene dosage, with heterozygotes having an intermediate phenotype. Fasciculation of ipRGCs and Mito-Y-positive RGCs precedes changes in cell number and is not solely the result of increased cell density. A fasciculation phenotype is not observed in *Bax*-deficient retinas at P0, in which normal developmental cell death is inhibited (Figures S10B–S10G), suggesting that fasciculation is not a secondary result of *Dscam* deficiency. Other mechanisms may contribute, such as an interaction with DCC, which may function as a dependence receptor as well as a NETRIN receptor, but changes in synaptic activity, target derived trophism, and other mechanisms may also be involved.

Therefore, our conclusion from studying DSCAM and DSCAML1 in multiple cells types in the mouse retina is that these proteins function similarly in self-avoidance by masking cell-type-intrinsic adhesion. We do not observe an essential role for these proteins in the stratification of processes in the inner plexiform layer, or in synaptic specificity where we have been able to evaluate these functions. The gene expression patterns and overt phenotypes of *Dscam* and *Dscaml1* mutant mice make it clear that their functions extend beyond the retina, and DSCAMs may serve other roles in other cell types elsewhere in the nervous system. It will be important to determine whether their role in other regions of the CNS is also limited to self-avoidance, and how these roles relate to normal and abnormal neurodevelopment.

EXPERIMENTAL PROCEDURES

Mouse Strains

The following previously described mouse strains were used in this study: Mito-Y: Tg(Eno2-YFP/Cox8a)YRwb/J (Misgeld et al., 2007), $Dscam^{-/-}$: B6.CBy-($Dscam^{del17}$)/RwbJ, and *Bax*-deficient mice: B6.129X1-(Bax^{tm1Sjk})/J (Jax stock 002994). Mice were used in accordance with protocols approved by the Animal Care and Use Committee at The Jackson Laboratory.

RNA In Situ Hybridization

Fluorescent in situ hybridization was performed as previously described (Fuerst et al., 2008). For colorimetric RNA in situ hybridization, the *Dscam* template for riboprobe synthesis was generated by subcloning an ~800 bp fragment corresponding to nucleotides 4642–5428 of mouse *Dscam* into pBluescript KS+. In situ hybridization, using digoxigenin (DIG)-labeled riboprobes was performed on 100 μm sections of E12.5–E17.5 embryonic mouse heads as previously described (Erskine et al., 2000). Briefly, sections were dehydrated and rehydrated in 25%–100% methanol in PBT (PBS + 0.1% Tween-20), bleached with 6% H_2O_2 (Sigma-Aldrich, Dorset, UK) in PBT for 1 hr, treated with 5 μg/ml Proteinase K (Sigma-Aldrich) in PBT for 5–10 min, followed by postfixation with 4% PFA in PBT. The sections were incubated at 65°C in hybridization buffer (50% Formamide, 5x SSC, 50 μg/ml tRNA, 1% SDS, 50 μg/ml heparin) for 1 hr, followed by hybridization overnight at 65°C. Sections were washed three times with 50% formamide, 5 x SSC, 1% SDS at 65°C, then with 50% formamide, 2 x SSC at 60°C, blocked with 10% sheep serum/TBST (TBS + 1% Tween-20) and incubated overnight in anti-DIG-alkaline phosphatase antibody (Roche Diagnostics, Lewes, UK) diluted 1:2000 in 1% sheep serum/TBST. To reveal the staining, the sections were washed with TBST followed by incubation in NBT (337.5 μg/ml, Sigma-Aldrich) and BCIP (175 μg/ml, Sigma-Aldrich) in NTMT (100 mM NaCl, 100 mM Tris-HCl,

pH 9.5, 50 mM MgCl2, 1% Tween-20). Identical staining was seen with probes raised to other regions of the gene. No staining was seen with the sense probe.

Dscaml1^{GT} Allele

The Sanger Genome Centre ES cell line CC0772 was used to generate the *Dscaml1*^{GT} mice. ES cells were injected into blastocysts and resulting male chimeras were bred to C57BL/6J females. Offspring were PCR-genotyped for the *β-gal* cassette using the primers β-gal F (atc ctc tgc atg gtc agg tc) and β-gal R (cgt ggc ctg att cat tcc) using 40 cycles of PCR with a 56°C annealing temperature. Pups carrying the gene trap were intercrossed, or backcrossed to C57BL/6J and genotyped by following the markers *D9MIT206* (CAT GCA CAT TTC CCC ACT G and TTT CTT TTC TTC CTT TTT CCC C) and *D9MIT129* (TTG TCT TTT AAC CTC CTG GAG C and TCC CAT CTT TCT CCT TGT GG), which flank the gene trap insertion and are polymorphic between C57BL/6J and 129/SvJ.

Northern Blot Analysis

Northern blot analysis was performed as previously described (Fuerst et al., 2007). Briefly, mRNA samples prepared from brains of P10 pups was polyA-purified using oligo d-T cellulose (Sigma-Aldrich) and run on a formaldehyde agarose gel and transferred to a nylon membrane. Primers 5′ of the gene trap, Dscaml1NF (tgc tcc tgg act ctt tac aca) and Dscaml1NR (ctg gag tga tgg aga ccg tg), were used to amplify a probe including sequence from exons 1–3. The PCR-derived probe was labeled with ^{32}P using a Rediprime II labeling kit (GE Healthcare; RPN1633) and hybridized to the membrane. The membrane was washed and developed.

β-Gal Assay

Mice were transcardially perfused with 4% PFA, brains and retinas were dissected out and immersion fixed in 4% PFA for 24 hr. 50 μm sections were cut using a vibratome and stained with 4 mM potassium ferricyanate, 4 mM potassium ferrocyanate, 2 mM $MgCl_2$, and 0.8 mg/ml X-gal. Tissue sections were stained for 24 hr to 48 hr at 30°C. Tissue was rinsed in PBS and counterstained with DAPI. Images were generated using a bright-field image of the X-gal precipitate and a fluorescent image of DAPI, which was made negative and superimposed on the blue X-gal staining.

Immunohistochemistry

Enucleated eyes were fixed in 4% paraformaldehyde overnight. Tissue was equilibrated in 30% sucrose/PBS and frozen in OCT media. 10 μm sections were blocked in 3% normal donkey serum in 1x PBS and 0.1% triton. Primary antibodies were incubated overnight at 4°C and subsequently washed 2 times for 10 min in PBS. Sections were incubated at room temperature with secondary antibodies for 1 hr, and then washed four times in PBS for 10 min. The last wash contained 2 μl of 1 mg/ml Dapi per 40 ml PBS.

Whole Retina Staining

Mice were transcardially perfused with PBS and 4% paraformaldehyde. Eyes were enucleated and placed in PBS. A small hole was made at the junction between the ciliary body and retina with a 30 gauge needle. The eye was hemisected and the retina was teased away from the sclera. Retinas were fixed a second time in 4% paraformaldehyde overnight, followed by a rinse in PBS and incubation with primary antibodies in PBS containing 3% normal horse serum and 0.5% Triton-X 100, for 3–5 days at 4°C, with gentle rocking. Retinas were washed overnight in PBS and labeled with secondary antibodies in PBS, 3% normal horse serum and 0.5% triton. Retinas were washed for 2–4 hr in PBS and flat mounted in an antifade media. All fluorescent images were acquired on a Leica SP5 confocal microscope.

Antibodies

The following antibodies were used in this study: goat anti-DSCAML1 (R&D Systems, AF3315 at 1:200), generated against the entire extracellular domain of human DSCAML1, Smi-32 mouse anti-non-phosphorylated neurofilament (Covance, SMI-32R at 1:500), rabbit anti-melanopsin (generously gift of Ignacio Provencio, Uniformed Services University of the Health Sciences, at 1:10,000), mouse anti-tyrosine hydroxylase (Novocastra, NCL-TH at 1:25), rabbit anti-tyrosine hydroxylase (Millipore, AB152 at 1:500), goat anti-ChAT (Millipore, AB144P at 1:500) rabbit anti-β-gal (Eppendorf at 1:500), rabbit anti-PKCα (Sigma-aldrich, P4334 at 1:10,000), mouse anti-PKCα (Santa Cruz Biotechnology, SC8393 at 1:500), rabbit anti-disabled (generous gift of Dr. Brian Howell, at 1:500), mouse anti-CTBP2 (BD biosciences, 612044 at 1:500), chicken anti-β-gal (Abcam, ab7 at 1:100), rabbit anti-NK3 (Abcam, ab7 at 1:200), rabbit anti-calsenilin (Abcam, ab9661770 at 1:200), rat anti-HCN4 (Abcam, ab 32675 at 1:50), rabbit anti-calbindin (Chemicon, D-28K at 1:400) and mouse anti-SYT2 (ZIRC, ZNP-1 at 1:400), rabbit anti-BRN3A (Millipore UK, ab5945 at 1:500), mouse anti-TUJ1 (Cambridge Bioscience Ltd at 1:1000) and mouse anti-dystroglycan (DSHB, clone MANDAG at 1:500), goat anti-ChAT (Millipore, AB144P at 1:500), goat anti-BRN3B (Santa Cruz Biotechnology, 6026 at 1:400), mouse anti-cacna1s (Millipore, MAB427 at 1:400) rabbit anti-PAK1 S144^{P}, S199^{P} and T423^{P} (Cell Signaling Technology at 1:500) and mouse anti-PAK1 T212^{P} (Sigma-Aldrich at 1:500).

Electron Microscopy

Mice were transcardially perfused with 1.8% paraformaldehyde and 0.8% glutaraldehyde in phosphate buffer pH 7.2, after which retinas were dissected out and fixed overnight in the same fixative. Retinas were washed in PBS, and post fixed in 1% osmium tetroxide in 0.1 M PBS for 4 hr at 4°C followed by two 15 min washes in PBS. Retinas were dehydrated in a series of ethanol and then incubated in propylene oxide for 20 min at room temperature. Retinas were then incubated in a 1:1 mixture of propylene oxide and epon-araldite for 24 hr, followed by another 24 hr incubation in 100% epon-araldite. Retinas were cured at 65°C for 3 days, cut, and imaged.

Density Recovery Profile Analysis

DRP analysis was performed as previously described (Rockhill et al., 2000; Rodieck, 1991). 1.55 mm sections of wild-type and *Dscaml1*$^{GT/GT}$ retinas stained with antibodies to TH were used to measure the DRP of DA cells (n = 4 for each genotype). 0.775 mm sections of wild-type and *Dscaml1*$^{GT/GT}$ retinas stained with antibodies to DAB1 were used to measure the DRP of AII cells (n = 3 for each genotype). Mito-Y retinas were imaged and montaged for analysis (n = 3 for each genotype). The dorsal portion of the Mito-Y retina was not included in the DRP analysis. In all cases, the first bin was discarded to account for the soma size.

Bipolar-AII paired recordings

Electrophysiological experiments were performed in an in vitro slice preparation of retina isolated from light-adapted *Dscaml1*$^{GT/GT}$ and C57BL/6 (wild-type) mice aged P25–P35. Following induction of isofluorane, mice were decapitated and eyes removed into cool (~10°C) Ames' medium (Sigma) with $NaHCO_3$ (23 mM) added (gassed with 95% O_2/5% CO_2, called Carbogen). Retinas were isolated and small pieces of retina embedded in low melting point agarose (3%; Sigma Type VII-A) in a solution containing (in mM) 119 NaCl, 40 HEPES, 1.25 NaH_2PO_4, 2.5 KCl, 2.5 $CaCl_2$, and 1.5 $MgSO_4$ (pH = 7.4 with NaOH). The agarose block was cut with a vibratome in 200 μm transverse sections while submerged in gassed Ames' medium.

Retinal slices were placed in a Plexiglas chamber and superfused at ~1 ml/min with artificial cerebrospinal fluid (ACSF) gassed with Carbogen and containing (in mM) 119 NaCl, 23 $NaHCO_3$,10 glucose, 1.25 NaH_2PO4, 2.5 KCl, 1.1 $CaCl_2$, 1.5 $MgSO_4$, 2 Na lactate, and 2 Na pyruvate (osmolarity ≈290 mOsm), at near-physiological temperature (~35°C). The ACSF contained picrotoxin (100 μM), TPMPA (50 μM), strychnine (0.5 μM), tetrodotoxin (TTX, 0.25 μM), L-AP4 (2 μM), and niflumic acid (50 μM) to block GABAAR-, GABACR-, glycine receptor-, voltage-gated Na channel-mediated, mGluR6-linked, and Ca-activated Cl currents, respectively. All drugs and chemicals were obtained from Sigma or Tocris (except for TTX from Alamone Labs).

Whole-cell voltage-clamp recordings were made from visualized neurons using pipettes (~5 MΩ) containing (in mM) 90 $CsCH_3SO_3$, 20 TEA-Cl, 20 HEPES, 1 BAPTA, 8 tris-phosphocreatine, 4 MgATP, 0.4 NaGTP, and 0.2 mM Alexa hydrazide 488 or 564 tracer for visualization of recorded cells' morphologies (pH = 7.3 by CsOH, osmolarity adjusted to 280 mOsm with sucrose). All access resistance (R_{access}) was <20 MΩ, compensated 50%–90%; RB R_{access} < 40 MΩ and not compensated.

Recordings were made using MultiClamp 700A or 700B amplifiers (Axon Instruments). Signals were low-pass filtered by the amplifier (2–10 kHz) and

digitized (10–50 kHz) by an Instrutech ITC-18 A/D board (Instrutech) controlled by Igor Pro software (WaveMetrics). To elicit presynaptic Ca currents, voltage steps are applied to neurons; a P/4 leak subtraction protocol was used to eliminate leak currents. Data analysis was performed using Igor Pro. ANOVA was used to judge the significance of differences in unpaired data sets. Significance was accepted when $p < 0.05$.

Electroretinography

Dark-adapted electroretinograms were recorded as previously described (Haider et al., 2008). Mice were dark adapted for at least 6 hr before being anesthetized. Electroretinograms (ERGs) were recorded from the corneal surface of one eye after pupil dilation.

SUPPLEMENTAL DATA

Supplemental Data include ten figures and Supplemental Experimental Procedures and can be found with this article online at http://www.cell.com/neuron/supplemental/S0896-6273(09)00738-7.

ACKNOWLEDGMENTS

We would like to thank Dr. Brian Howell for the anti-disabled1 antibody, Dr. Ignacio Provencio for the melanopsin antibody, Drs. Zhong-wei Zhang and Susan Ackerman for comments on the manuscript, and Dr. Ben Reese for helpful discussions. We would also like to thank the Scientific Services at The Jackson Laboratory. This work was supported by grants from the National Institutes of Health (EY018605 to R.W.B.) and the Knights Templar Eye Research Foundation (P.G.F.). The Scientific Services at Jackson are supported by CA034196. F.B. is a recipient of a BBSRC studentship.

Accepted: September 9, 2009
Published: November 25, 2009

REFERENCES

Agarwala, K.L., Ganesh, S., Tsutsumi, Y., Suzuki, T., Amano, K., and Yamakawa, K. (2001). Cloning and functional characterization of DSCAML1, a novel DSCAM-like cell adhesion molecule that mediates homophilic intercellular adhesion. Biochem. Biophys. Res. Commun. *285*, 760–772.

Amano, K., Fujii, M., Arata, S., Tojima, T., Ogawa, M., Morita, N., Shimohata, A., Furuichi, T., Itohara, S., Kamiguchi, H., et al. (2009). DSCAM deficiency causes loss of pre-inspiratory neuron synchroneity and perinatal death. J. Neurosci. *29*, 2984–2996.

Andrews, G.L., Tanglao, S., Farmer, W.T., Morin, S., Brotman, S., Berberoglu, M.A., Price, H., Fernandez, G.C., Mastick, G.S., Charron, F., and Kidd, T. (2008). Dscam guides embryonic axons by Netrin-dependent and -independent functions. Development *135*, 3839–3848.

Chen, B.E., Kondo, M., Garnier, A., Watson, F.L., Puettmann-Holgado, R., Lamar, D.R., and Schmucker, D. (2006). The molecular diversity of Dscam is functionally required for neuronal wiring specificity in Drosophila. Cell *125*, 607–620.

Coombs, J., van der List, D., Wang, G.Y., and Chalupa, L.M. (2006). Morphological properties of mouse retinal ganglion cells. Neuroscience *140*, 123–136.

Erskine, L., Williams, S.E., Brose, K., Kidd, T., Rachel, R.A., Goodman, C.S., Tessier-Lavigne, M., and Mason, C.A. (2000). Retinal ganglion cell axon guidance in the mouse optic chiasm: expression and function of robos and slits. J. Neurosci. *20*, 4975–4982.

Fuerst, P.G., Rauch, S.M., and Burgess, R.W. (2007). Defects in eye development in transgenic mice overexpressing the heparan sulfate proteoglycan agrin. Dev. Biol. *303*, 165–180.

Fuerst, P.G., Koizumi, A., Masland, R.H., and Burgess, R.W. (2008). Neurite arborization and mosaic spacing in the mouse retina require DSCAM. Nature *451*, 470–474.

Galli-Resta, L., Leone, P., Bottari, D., Ensini, M., Rigosi, E., and Novelli, E. (2008). The genesis of retinal architecture: An emerging role for mechanical interactions? Prog. Retin. Eye Res. *27*, 260–283.

Haider, N.B., Zhang, W., Hurd, R., Ikeda, A., Nystuen, A.M., Naggert, J.K., and Nishina, P.M. (2008). Mapping of genetic modifiers of Nr2e3 rd7/rd7 that suppress retinal degeneration and restore blue cone cells to normal quantity. Mamm. Genome *19*, 145–154.

Hattori, D., Demir, E., Kim, H.W., Viragh, E., Zipursky, S.L., and Dickson, B.J. (2007). Dscam diversity is essential for neuronal wiring and self-recognition. Nature *449*, 223–227.

Hattori, D., Millard, S.S., Wojtowicz, W.M., and Zipursky, S.L. (2008). Dscam-mediated cell recognition regulates neural circuit formation. Annu. Rev. Cell Dev. Biol. *24*, 597–620.

Hughes, M.E., Bortnick, R., Tsubouchi, A., Baumer, P., Kondo, M., Uemura, T., and Schmucker, D. (2007). Homophilic Dscam interactions control complex dendrite morphogenesis. Neuron *54*, 417–427.

Hummel, T., Vasconcelos, M.L., Clemens, J.C., Fishilevich, Y., Vosshall, L.B., and Zipursky, S.L. (2003). Axonal targeting of olfactory receptor neurons in Drosophila is controlled by Dscam. Neuron *37*, 221–231.

Li, W., and Guan, K.L. (2004). The Down syndrome cell adhesion molecule (DSCAM) interacts with and activates Pak. J. Biol. Chem. *279*, 32824–32831.

Li, H.L., Huang, B.S., Vishwasrao, H., Sutedja, N., Chen, W., Jin, I., Hawkins, R.D., Bailey, C.H., and Kandel, E.R. (2009). Dscam mediates remodeling of glutamate receptors in Aplysia during de novo and learning-related synapse formation. Neuron *61*, 527–540.

Liu, G., Li, W., Wang, L., Kar, A., Guan, K.L., Rao, Y., and Wu, J.Y. (2009). DSCAM functions as a netrin receptor in commissural axon pathfinding. Proc. Natl. Acad. Sci. USA *106*, 2951–2956.

Ly, A., Nikolaev, A., Suresh, G., Zheng, Y., Tessier-Lavigne, M., and Stein, E. (2008). DSCAM is a netrin receptor that collaborates with DCC in mediating turning responses to netrin-1. Cell *133*, 1241–1254.

Masland, R.H. (2001). Neuronal diversity in the retina. Curr. Opin. Neurobiol. *11*, 431–436.

Matthews, B.J., Kim, M.E., Flanagan, J.J., Hattori, D., Clemens, J.C., Zipursky, S.L., and Grueber, W.B. (2007). Dendrite self-avoidance is controlled by Dscam. Cell *129*, 593–604.

Millard, S.S., Flanagan, J.J., Pappu, K.S., Wu, W., and Zipursky, S.L. (2007). Dscam2 mediates axonal tiling in the Drosophila visual system. Nature *447*, 720–724.

Misgeld, T., Kerschensteiner, M., Bareyre, F.M., Burgess, R.W., and Lichtman, J.W. (2007). Imaging axonal transport of mitochondria in vivo. Nat. Methods *4*, 559–561.

Neves, G., and Chess, A. (2004). Dscam-mediated self- versus non-self-recognition by individual neurons. Cold Spring Harb. Symp. Quant. Biol. *69*, 485–488.

Neves, G., Zucker, J., Daly, M., and Chess, A. (2004). Stochastic yet biased expression of multiple Dscam splice variants by individual cells. Nat. Genet. *36*, 240–246.

Panda, S., Sato, T.K., Castrucci, A.M., Rollag, M.D., DeGrip, W.J., Hogenesch, J.B., Provencio, I., and Kay, S.A. (2002). Melanopsin (Opn4) requirement for normal light-induced circadian phase shifting. Science (New York, N. Y *298*, 2213–2216.

Raviola, E., and Dacheux, R.F. (1987). Excitatory dyad synapse in rabbit retina. Proc. Natl. Acad. Sci. USA *84*, 7324–7328.

Rockhill, R.L., Euler, T., and Masland, R.H. (2000). Spatial order within but not between types of retinal neurons. Proc. Natl. Acad. Sci. USA *97*, 2303–2307.

Rodieck, R.W. (1991). The density recovery profile: a method for the analysis of points in the plane applicable to retinal studies. Vis. Neurosci. *6*, 95–111.

Sanes, J.R., and Yamagata, M. (2009). Many paths to synaptic specificity. Annu. Rev. Cell Dev. Biol. *25*, 161–195.

Schmidt, T.M., and Kofuji, P. (2009). Functional and morphological differences among intrinsically photosensitive retinal ganglion cells. J. Neurosci. *29*, 476–482.

Schmucker, D., and Chen, B. (2009). Dscam and DSCAM: complex genes in simple animals, complex animals yet simple genes. Genes Dev. *23*, 147–156.

Schmucker, D., Clemens, J.C., Shu, H., Worby, C.A., Xiao, J., Muda, M., Dixon, J.E., and Zipursky, S.L. (2000). Drosophila Dscam is an axon guidance receptor exhibiting extraordinary molecular diversity. Cell *101*, 671–684.

Singer, J.H., and Diamond, J.S. (2006). Vesicle depletion and synaptic depression at a mammalian ribbon synapse. J. Neurophysiol. *95*, 3191–3198.

Soba, P., Zhu, S., Emoto, K., Younger, S., Yang, S.J., Yu, H.H., Lee, T., Jan, L.Y., and Jan, Y.N. (2007). Drosophila sensory neurons require Dscam for dendritic self-avoidance and proper dendritic field organization. Neuron *54*, 403–416.

Viney, T.J., Balint, K., Hillier, D., Siegert, S., Boldogkoi, Z., Enquist, L.W., Meister, M., Cepko, C.L., and Roska, B. (2007). Local retinal circuits of melanopsin-containing ganglion cells identified by transsynaptic viral tracing. Curr. Biol. *17*, 981–988.

Wang, J., Zugates, C.T., Liang, I.H., Lee, C.H., and Lee, T. (2002). Drosophila Dscam is required for divergent segregation of sister branches and suppresses ectopic bifurcation of axons. Neuron *33*, 559–571.

Wang, J., Ma, X., Yang, J.S., Zheng, X., Zugates, C.T., Lee, C.H., and Lee, T. (2004). Transmembrane/juxtamembrane domain-dependent Dscam distribution and function during mushroom body neuronal morphogenesis. Neuron *43*, 663–672.

Wassle, H., Puller, C., Muller, F., and Haverkamp, S. (2009). Cone contacts, mosaics, and territories of bipolar cells in the mouse retina. J. Neurosci. *29*, 106–117.

Whitney, I.E., Raven, M.A., Ciobanu, D.C., Williams, R.W., and Reese, B.E. (2009). Multiple genes on chromosome 7 regulate dopaminergic amacrine cell number in the mouse retina. Invest. Ophthalmol. Vis. Sci. *50*, 1996–2003.

Wojtowicz, W.M., Flanagan, J.J., Millard, S.S., Zipursky, S.L., and Clemens, J.C. (2004). Alternative splicing of Drosophila Dscam generates axon guidance receptors that exhibit isoform-specific homophilic binding. Cell *118*, 619–633.

Wojtowicz, W.M., Wu, W., Andre, I., Qian, B., Baker, D., and Zipursky, S.L. (2007). A vast repertoire of dscam binding specificities arises from modular interactions of variable Ig domains. Cell *130*, 1134–1145.

Yamagata, M., and Sanes, J.R. (2008). Dscam and Sidekick proteins direct lamina-specific synaptic connections in vertebrate retina. Nature *451*, 465–469.

Yamagata, M., Weiner, J.A., and Sanes, J.R. (2002). Sidekicks: synaptic adhesion molecules that promote lamina-specific connectivity in the retina. Cell *110*, 649–660.

Yamakawa, K., Huot, Y.K., Haendelt, M.A., Hubert, R., Chen, X.N., Lyons, G.E., and Korenberg, J.R. (1998). DSCAM: a novel member of the immunoglobulin superfamily maps in a Down syndrome region and is involved in the development of the nervous system. Hum. Mol. Genet. *7*, 227–237.

Zhan, X.L., Clemens, J.C., Neves, G., Hattori, D., Flanagan, J.J., Hummel, T., Vasconcelos, M.L., Chess, A., and Zipursky, S.L. (2004). Analysis of Dscam diversity in regulating axon guidance in Drosophila mushroom bodies. Neuron *43*, 673–686.

Zhang, D.Q., Wong, K.Y., Sollars, P.J., Berson, D.M., Pickard, G.E., and McMahon, D.G. (2008). Intraretinal signaling by ganglion cell photoreceptors to dopaminergic amacrine neurons. Proc. Natl. Acad. Sci. USA *105*, 14181–14186.

Zhu, H., Hummel, T., Clemens, J.C., Berdnik, D., Zipursky, S.L., and Luo, L. (2006). Dendritic patterning by Dscam and synaptic partner matching in the Drosophila antennal lobe. Nat. Neurosci. *9*, 349–355.